Effects of Mutations in Apolipoprotein C-1 on the Reconstitution and Kinetic Stability of Discoidal Lipoproteins†

Ranjana Mehta,‡ Donald L. Gantz, and Olga Gursky*

Department of Physiology and Biophysics, Boston University School of Medicine, W329, 715 Albany Street, Boston, Massachusetts 02118

Received January 22, 2003; Revised Manuscript Received March 6, 2003

ABSTRACT: To probe the role of protein conformation in the formation and kinetic stability of discoidal lipoproteins, thermal unfolding and refolding studies were carried out using model lipoproteins reconstituted from dimyristoylphosphatidylcholine (DMPC) and selected mutants of human apolipoprotein C-1 (apoC-1). Circular dichroism (CD) spectroscopy and electron microscopy show that the Q31P mutant, which has α-helical content in solution (33%) and on DMPC disks (67%) similar to that of the wild type (WT), forms disks of smaller diameter, $\langle d \rangle = 13$ nm, compared to 17 nm of the WT−DMPC disks. The L34P mutant, which is largely unfolded in solution, forms disks with α-helix content and diameter similar to those of the WT. The R23P mutant, which is fully unfolded in solution, forms disks that have similar diameter but reduced α-helix content (40%) compared to the WT−DMPC disks (65%). Remarkably, despite large variations in the α-helix content or the disk diameter among different mutant−DMPC complexes, the mutations have no significant effect on the unfolding rates or the Arrhenius activation energy of the disk denaturation, $E_a = 25-29$ kcal/mol. This suggests that the kinetic stability of the discoidal complexes is dominated by the lipid−lipid rather than the protein−lipid interactions. In contrast to the heat denaturation, the lipoprotein reconstitution upon cooling monitored by CD and light scattering is significantly affected by mutations, with Q31P forming disks in the broadest and R23P in the narrowest temperature range. Our results suggest that the apolipoprotein helical structure in solution facilitates reconstitution of discoidal lipoproteins but has no significant effect on their kinetic stability.

Lipids in plasma are transported in the form of lipoproteins that are heterogeneous assemblies of specific proteins (termed apolipoproteins) and lipids. Lipoproteins are classified according to their size, density, protein and lipid composition, and metabolic properties into several major groups, including high-density, low-density, and very low density lipoproteins (HDL,[1] LDL, and VLDL, respectively) and chylomicrons (*1*, *2*). Our focus is on HDL whose well-established antiatherogenic function is mediated via the receptor-mediated cholesterol removal from peripheral tissue to the liver (*1*−*5*) and via the antioxidant action of HDL on LDL (*6*). Nascent hepatic HDL form phospholipid bilayer disks with proteins wrapped around the disk circumference (Figure 1A). The apolar faces of the apolipoprotein amphipathic α-helices interact with phospholipids, and the polar faces are exposed to solvent (*7*), thereby conferring the disk solubility. These nascent discoidal HDL acquire cholesterol from the tissue cells and are converted to mature spherical HDL by the action of lecithin:cholesterol acyltransferase (LCAT) (reviewed in refs *4* and *8*). Our aim is to obtain the molecular determinants for the structural stability of the heterogeneous HDL particles.

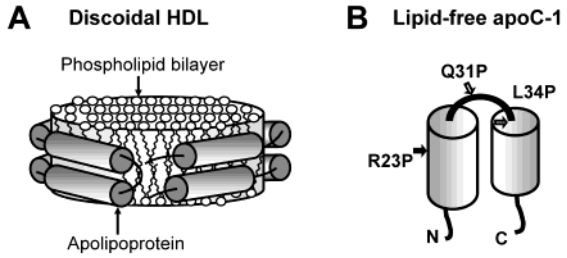

FIGURE 1: Cartoon representation of the discoidal lipoprotein assembly (A) and solution conformation of lipid-free apoC-1 (B). Protein α-helices are shown by cylinders. The sites of Pro substitutions used are indicated.

Structural stability is essential for HDL functions in lipid transport and metabolism and in the pathogenesis of atherosclerosis and hypertriglyceridemia (*9*), yet molecular mechanisms of lipoprotein stabilization are not clearly understood. Most existing reports on lipoprotein stability are based upon the equilibrium thermodynamic approach (for recent reviews see refs *9*−*15*). However, our recent analyses of model discoidal HDL (*16*) and spherical human plasma HDL (*17*), supported by several earlier studies (*18*−*20*), have shown that, contrary to the widely held assumption, HDL stability has a kinetic rather than a thermodynamic origin. High

† This work was supported by National Institutes of Health Grant GM67260 to O.G. Support for the CD spectroscopy and electron microscopy core facilities comes from NIH Program Project Grant HL26355 (David Atkinson, Principal Investigator).

* Corresponding author. E-mail: gursky@biophysics.bumc.bu.edu. Phone: (617) 638-7894. Fax: (617) 638-4041.

‡ Current address: Department of Medicinal Chemistry, Box 357610, School of Pharmacy, University of Washington, Seattle, WA 98195.

[1] Abbreviations: HDL, high-density lipoprotein; LDL, low-density lipoprotein; VLDL, very low density lipoprotein; LCAT, lecithin: cholesterol acyltransferase; apoC-1, apolipoprotein C-1; WT, wild-type protein; DMPC, dimyristoylphosphatidylcholine; CD, circular dichroism spectroscopy; EM, electron microscopy; T-jump, temperature jump.

10.1021/bi0341253 CCC: $25.00 © 2003 American Chemical Society
Published on Web 04/03/2003

kinetic barriers for lipoprotein disintegration, $\Delta G^* \sim 16-17$ kcal/mol, may facilitate lipoprotein stability in the absence of high packing specificity and slow spontaneous interconversions among lipoproteins from different subclasses, thereby modulating lipoprotein lifetime and functions (*16*, *17*). By correlating circular dichroism (CD) spectroscopic data with the light scattering and electron microscopic (EM) data, we showed that the protein unfolding on HDL is coupled to particle fusion, which compensates for the energetically unfavorable solvent exposure of the apolar lipid surface upon apolipoprotein unfolding. On the basis of this coupling we proposed that the high kinetic barrier for the HDL denaturation originates from the transient disruption of lipid−lipid and/or lipid−protein packing interactions in the course of lipoprotein fusion (*16*).

In this work, we test the role of protein conformation in the kinetic stability of discoidal HDL. To do so, we use reconstituted model lipoproteins comprised of a neutral phospholipid, dimyristoylphosphatidylcholine (DMPC), and selected mutants of human apolipoprotein C-1 (apoC-1). ApoC-1, which is the smallest exchangeable apolipoprotein (6 kDa), is a constituent of HDL and VLDL and an important factor in lipoprotein metabolism (*21*, *22*). ApoC-1 on nascent HDL is a potent LCAT activator (*23*), a function that is reproduced on the disks reconstituted from apoC-1, phosphatidylcholine, and cholesterol (*24*). The amino acid sequence of apoC-1, similar to those of other exchangeable apolipoproteins, is comprised of 11-mer tandem repeats that are predicted to fold into characteristic amphipathic α-helices (*7*). ApoC-1 contains four such repeats spanning residues 7−51 that are predicted to form two α-helices, 7−32 and 33−53 (*7*). Consistent with this prediction, the NMR structure of apoC-1 on "lipid-mimicking" SDS micelles shows two helices, 7−29 and 38−52 (*25*). The helical content of apoC-1 is reduced from 65% on lipoproteins to an average of 31% α-helix and ∼65% random coil in the monomeric lipid-free state in solution (*26*). Our spectroscopic and mutagenesis studies have shown that apoC-1 in solution adopts a dynamic helix−turn−helix conformation that may represent a minimal folding unit in other exchangeable apolipoproteins (*27*, *28*) (Figure 1B). This result, together with the high amino acid sequence homology and the structural and functional similarity of apoC-1 and larger apolipoproteins, makes apoC-1 an excellent model for the analysis of the energetics−structure−function relationship in this protein family.

To analyze, in the context of a single protein, the effects of the apolipoprotein conformation on the reconstitution and kinetic stability of discoidal lipoproteins, we use three apoC-1 mutants containing single Pro substitutions that have distinctly different effects on the protein structure in solution (*28*) (Figure 1B). The R23 → P mutation at an internal site of the N-terminal α-helix leads to a complete unfolding of the lipid-free solution conformation (<5% α-helix, >85% random coil). In contrast, the Q31 → P mutation in the interhelical linker is well tolerated and causes no protein unfolding or destabilization in solution. The L34 → P mutation near the start position of the C-terminal helix induces substantial protein unfolding in solution (10% α-helix, >80% random coil). Here, we determine the effects of these mutations on the apoC-1−DMPC disk structure, thermal stability, and reconstitution by using CD spectroscopy in conjunction with light scattering and electron microscopy (EM). The results provide an insight into the role of protein conformation in the reconstitution and stability of discoidal HDL and into the nature of the rate-limiting transition state in lipoprotein denaturation.

MATERIALS AND METHODS

Lipoprotein Preparation and Imaging. Mutant forms of full-size human apoC-1 (57 amino acids) containing single Pro substitutions at selected sites, R23 → P, Q31 → P, and L34 → P, were obtained by solid-state synthesis and purified to 98%+ purity as described (*27*). Protein−DMPC complexes were prepared as described using a protein:lipid ratio of 1:4.5 to 1:5 mg/mg (*16*). Briefly, 1 mg/mL solution of lyophilized protein in 5 mM sodium phosphate buffer, pH 7.6−7.8, was incubated at room temperature with a suspension of ultrapure DMPC liposomes (Sigma) in the same buffer. The mixture of Q31P−DMPC cleared in about 20 min; however, liposome clearance by L34P and, especially, R23P appeared slower and took 1−3 h. After overnight incubation, the samples were diluted by buffer to final protein concentration of 10−30 μg/mL and were used in CD spectroscopic and electron microscopic experiments within 2 weeks. Attempts to reconstitute lipoproteins at 36 °C led to liposome clearance and discoidal complex formation with Q31P but not with other mutants.

Protein−lipid complexes were visualized by the negative staining technique in a CM12 transmission electron microscope (Philips Electron Optics) as described (*16*). Statistical analysis of the disk size distribution was carried out using at least 200 particles per image and utilizing the EXCEL program. All electron microscopic experiments were repeated three to four times to ensure reproducibility.

Circular Dichroism Spectroscopy and Light Scattering. CD and dynode voltage data (the latter report on the changes in the light scattering by lipoprotein disks) were recorded as described (*16*) using an upgraded AVIV 62DS spectrometer equipped with a thermoelectric temperature control. Briefly, far-UV CD spectra, melting, and kinetic data were recorded from lipoprotein solutions of 10−30 μg/mL protein concentration placed in 5 mm or 10 mm quartz cells. The CD and dynode voltage melting data, $\Theta_{222}(T)$ and $V_{222}(T)$, were recorded at 222 nm upon sample heating and cooling from 25 to 85 °C at a constant rate from 0.067 to 1.34 K/min. Kinetic CD data, $\Theta_{222}(t)$, were recorded at 222 nm in temperature jump (T-jump) experiments in which the unfolding was induced by an abrupt increase in temperature from 25 to 45−85 °C. The dead time in these experiments was less than 2 min. All CD experiments were repeated three to six times to ensure reproducibility. Following the baseline subtraction, the CD data were normalized to the protein concentration and are expressed as molar residue ellipticity. Protein α-helical content was estimated from the normalized CD spectra as described (*16*). Normalized CD data were independent of the sample concentration in the range explored.

Kinetic Analysis. Thermal denaturation of apoC-1−DMPC complexes was analyzed by using a simple first-order Arrhenius kinetic model as described (*16*). Briefly, the unfolding rates $k(T)$ at 45−85 °C were determined by single-exponential approximation of the kinetic data, $\Theta_{222}(t)$, recorded by CD in T-jump experiments. The activation Gibbs

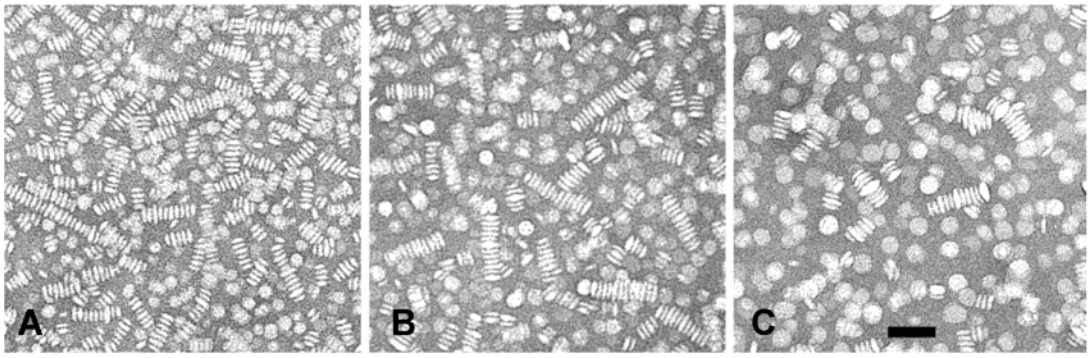

FIGURE 2: Electron micrographs of negatively stained discoidal lipoproteins reconstituted of mutant apoC-1 and DMPC. The images were recorded of DMPC complexes with Q31P (A), L34P (B), and R23P (C) that were prepared at 25 °C as described in Materials and Methods. The bar size is 50 nm.

free energy of unfolding, $\Delta G^* = G^* - G_F$, which is the difference between the free energies of the transition (*) and the folded (F) states, is related to the observed unfolding rate k via the modified Eyring equation (*29*):

$$\Delta G^* = -RT \ln(k/K) \quad (1)$$

Here, $R = 1.987$ cal/mol is the universal gas constant, T is temperature in kelvin, and K is the unfolding rate in the absence of the barrier that is assumed to be $K = 10^8$ s^{-1} (*30*, *31*).

The activation energy E_a for the lipoprotein disk denaturation, which approximates the enthalpic component ΔH^* of the free energy barrier $\Delta G^* = \Delta H^* - T\Delta S^*$, was determined from the slope of the Arrhenius plot, ln $k(T)$ versus $1/T$, using the reaction rates $k(T)$ measured in T-jump experiments. The accuracy in the determination of E_a, which incorporates the fitting errors and the deviations between repetitive experiments, is ±5 kcal/mol.

In addition, the value of E_a was assessed from the observed effects of the heating rate υ on the apparent melting temperature T_m (Figure 4) as described (*16*). This approach utilizes the relationship (*32*):

$$\ln(\upsilon/T_m^2) = \text{const} - E_a/RT_m \quad (2)$$

The value of E_a was determined from the slope of the plot $\ln(\upsilon/T_m^2)$ versus $1/T$ for each of the protein−lipid complexes analyzed in this work with an accuracy of ±5 kcal/mol that incorporates the fitting errors and the deviations among different data sets. The good agreement between this value of E_a and the activation energy determined from the Arrhenius plots confirms the consistency of our kinetic analysis.

RESULTS

Electron micrographs of the negatively stained complexes of apoC-1 mutants with DMPC show lipoprotein disks in a face-up orientation or stacked on edge in rouleaux (Figure 2). Such a disk stacking, which is an artifact of the negative staining, facilitates accurate disk size determination. The average disk diameters determined from the electron micrographs are 13.3 ± 2.5 nm for Q31P, 16.9 ± 2.5 nm for L34P, and 17.1 ± 2.5 nm for R23P. Thus, DMPC disks with R23P and L34P have diameters similar to that of the WT, $\langle d \rangle$ = 16.9 ± 2.7 nm (*16*), whereas Q31P forms significantly smaller disks.

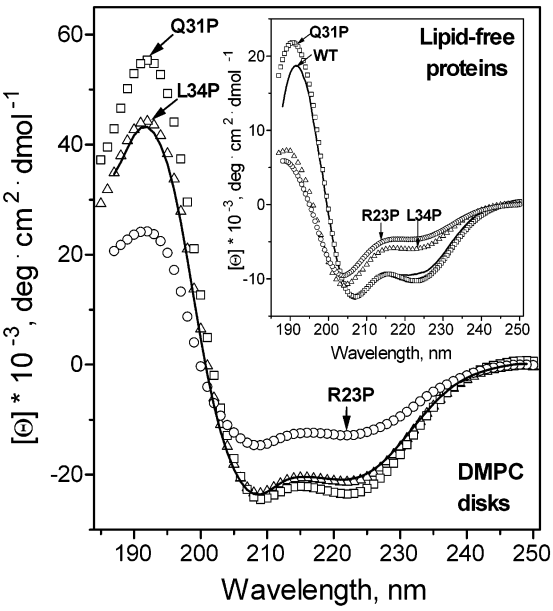

FIGURE 3: Far-UV CD spectra of mutant apoC-1−DMPC disks. The spectra of lipid-free proteins are shown in the insert for comparison. Key: (□) Q31P, (△) L34P, (○) R23P, and (—) WT.

Figure 3 shows far-UV CD spectra of the selected apoC-1 mutants in solution and in complex with DMPC, and Table 1 lists the α-helix content estimated from these spectra. The spectra of Q31P and WT largely overlap, suggesting that the helical content of Q31P in solution and on the lipid (33% and 67%, respectively) is similar or slightly higher than that of the WT (31% and 65%, respectively). Interestingly, L34P, which is largely unfolded in solution (<10% α-helix), in lipid complexes shows an α-helix content identical to that of the WT−DMPC disks, as indicated by complete superposition of the corresponding far-UV CD spectra (Figure 3, triangles and solid line). In contrast, R23P, which is unfolded in solution, shows only 40% helix content on the disks (Figure 3, circles), substantially lower than 65−67% in other apoC-1-containing disks. Thus, DMPC disks with R23P have similar diameters yet substantially lower helical content than those with WT or L34P. Furthermore, the disks containing Q31P have smaller diameter, yet their α-helix content is similar to that of the WT- or L34P-containing disks. In summary, our far-UV CD and EM data show that the protein helical content in solution or on the lipoprotein disks does not correlate with the disk diameter.

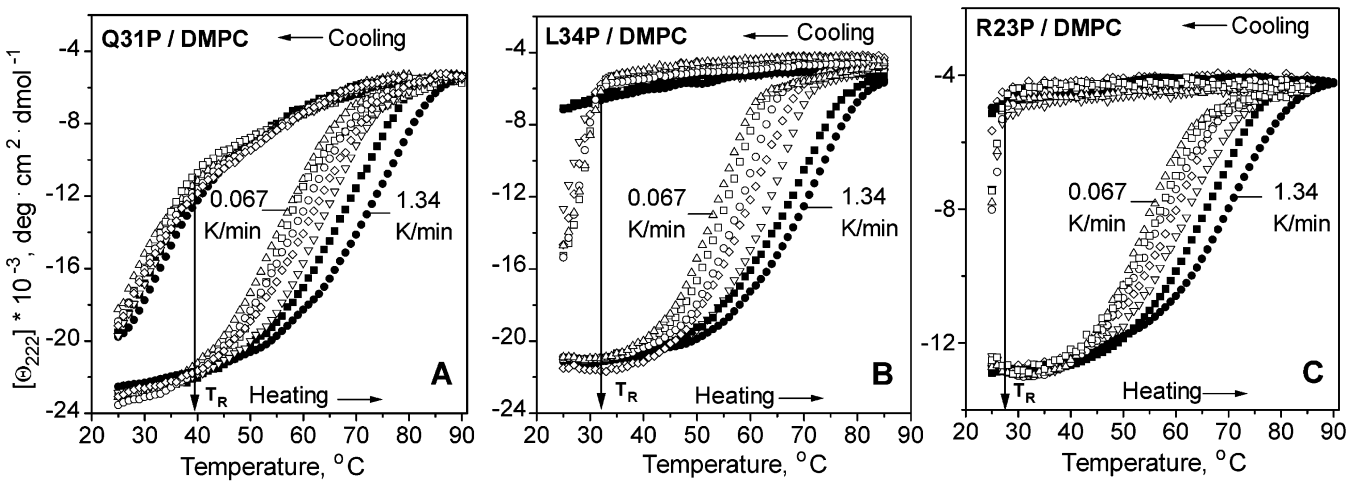

FIGURE 4: Thermal unfolding and refolding data of apoC-1 mutants on DMPC disks recorded by CD at various scan rates. Changes in the α-helical content of DMPC complexes with Q31P (A), L34P (B), and R23P (C) were monitored at 222 nm upon heating and consecutive cooling at various scan rates: (●) 1.34 K/min, (■) 0.76 K/min, (▽) 0.41 K/min, (◇) 0.18 K/min, (○) 0.12 K/min, (□) 0.092 K/min, and (△) 0.067 K/min.

Table 1: Structural and Energetic Parameters of Mutant ApoC-1 in Solution and in Complexes with DMPC[a]

	α-helix content[b] (%)				
protein	lipid free	on DMPC disks	disk diameter[c] ⟨*d*⟩ (nm)	E_a[d] (kcal/mol)	T_R[e] (°C)
WT	31	65	16.9	25	
Q31 → P	33	67	13.3	25.2	38
L34 → P	10	65	16.9	29.3	33
R23 → P	<5	40	17.1	25.8	27

[a] Parameters for the WT−DMPC complexes determined in ref *16* are listed for comparison. [b] Determined from the CD signal at 222 nm (Figure 3) with ±5% accuracy. [c] Average disk diameters were determined from electron micrographs in Figure 2; standard deviation is about 2.5 nm. [d] Activation energy E_a for the disk denaturation was determined from the slope of the Arrhenius plots in Figure 6 with an accuracy of ±5 kcal/mol. Similar values of E_a were obtained from the analysis of the scan rate effects on the apparent melting temperature (Figure 4) as described in ref *16*. [e] Highest temperature T_R of the disk reconstitution with DMPC was determined from the CD and/or dynode voltage cooling curves in Figures 4 and 5 with ±1.5 °C accuracy.

Figure 4 shows thermal unfolding and refolding data of the mutant apoC-1 on DMPC disks. These CD data were recorded upon sample heating and cooling at various constant rates from 0.067 to 1.34 K/min. Similar to the thermal unfolding of WT−DMPC disks (*16*), the unfolding data in Figure 4 show large scan rate dependence and display hysteresis at any scan rate explored, indicating a slow irreversible transition with high activation enthalpy and precluding equilibrium thermodynamic analysis of this transition. The heat unfolding curves in Figure 4 show a low-temperature shift by about 18 °C upon a reduction in the heating rate from 1.34 to 0.067 K/min; a similar shift was observed in the heat unfolding data of WT−DMPC disks (*16*). Quantitative analysis of the scan rate effects on the apparent melting temperature T_m by using the kinetic approach based on the Lumry−Eyring model (*32*) yielded the activation enthalpy $E_a = 25 \pm 5$ kcal/mol for the WT−DMPC disk denaturation (*16*); similar values of $E_a = 25 \pm 29$ kcal/mol for the mutant−DMPC disk denaturation were obtained from the kinetic analysis of the data in Figure 4. This suggests that, despite significant differences in their diameter or α-helical content, the DMPC disks containing WT and mutant apoC-1 have similar activation enthalpy of denaturation.

In contrast to the heat unfolding data, the refolding CD data recorded upon heating and consecutive cooling of apoC-1−DMPC complexes are significantly different for different mutants (Figure 4). The refolding curves of Q31P−DMPC disks (Figure 4A) are similar to those of the WT−DMPC disks but show less scan rate dependence (*16*). The gradual change in the CD signal in Figure 4A observed upon cooling from high temperatures to about 40 °C may be largely accounted for by the protein refolding in solution. However, the CD signal of the lipid-free Q31P monomer may not exceed $[\Theta_{222}(25\ °C)] \cong -10000$ deg·cm^2·dmol^{-1} (Figure 3, insert). Consequently, portions of the refolding curves below 40 °C showing a negative CD substantially larger than −10000 deg·cm^2·dmol^{-1} (Figure 4A) cannot be accounted for by the helical structure in lipid-free or lipid-poor protein and must reflect additional helical folding induced by the lipoprotein formation. Consistent with this interpretation, the first derivatives of the refolding curves in Figure 4A show an abrupt change in slope at about 40 °C (not shown), suggesting different mechanisms of protein refolding above and below 40 °C. Furthermore, electron micrographs taken after heating apoC-1−DMPC complexes to 85 °C followed by cooling to 25 °C show reconstituted lipoprotein disks (*16*). Taken together, these results suggest that cooling from 85 to 40 °C leads to refolding of the lipid-poor protein, while further cooling below 40 °C leads to Q31P−DMPC disk reconstitution and a concomitant folding of an additional helical structure.

The assignment of the highest temperature T_R of the protein−DMPC complex reconstitution to L34P and R23P is aided by the observation that these mutants are largely unfolded in solution but acquire helical structure on DMPC disks (Figure 3). At high temperatures, the CD signal of these mutants in the presence of DMPC is $[\Theta_{222}(25\ °C)] \sim -5000$ deg·cm^2·dmol^{-1} (Figure 4B,C), which is characteristic of the unfolded helical proteins. Upon cooling, the CD signal of R23P initially remains invariant in a broad temperature range, and the signal of L34P shows only a small gradual increase in intensity, consistent with the completely or largely

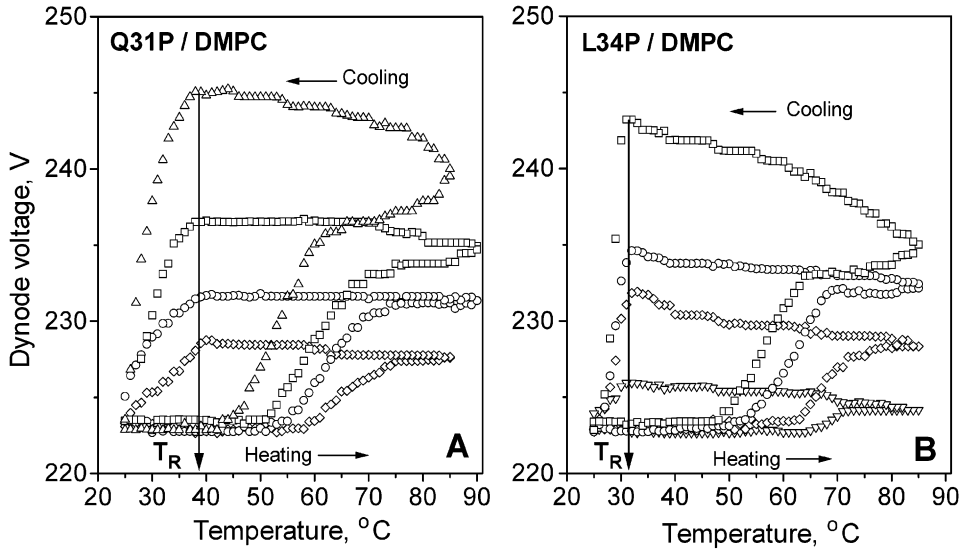

FIGURE 5: Thermally induced changes in the light scattering of lipoproteins monitored by dynode voltage: (A) Q31P and (B) L34P. The $V_{222}(T)$ data were recorded at 222 nm simultaneously with the $\Theta_{222}(T)$ data in Figure 4 upon heating and cooling at various rates. Line coding is same as in Figure 4.

unfolded solution conformation of R23P and L34P, respectively (*28*). However, cooling to lower temperatures at a rate $v \leq 0.41$ K/min leads to a steep increase in the negative CD in Figure 4B,C. Such a CD change, which is observed only in the presence of DMPC, must reflect an increase in the helical content induced by the protein−lipid association. The CD data in Figure 4B,C indicate that this DMPC-induced helical folding occurs at temperatures below $T_R = 33 \pm 1.5$ °C for L34P and below $T_R = 27 \pm 1.5$ °C for R23P.

The observed values of T_R for the apoC-1 mutants are independent of the cooling rate from 0.067 to 0.41 K/min (Figure 4B,C, open symbols). However, at faster scan rates of 0.76−1.34 K/min, the CD data recorded of L34P and R23P show no protein refolding on DMPC upon cooling to 25 °C (Figure 4B,C, solid symbols). This suggests that the cooling rates in these experiments are too fast for the lipid-induced protein refolding to be detected. Indeed, at 25 °C (close to the temperature $T_c = 24$ °C of the DMPC phase transition at which the disk formation is fastest), the apoC-1 refolding on DMPC occurs on a time scale of minutes (*16*). Therefore, the values of T_R for the protein refolding on DMPC can be experimentally determined only at relatively slow cooling rates, $v \leq 0.41$ K/min. At these slow scan rates, the independence of T_R of v or of the highest temperature of the sample exposure (that varied from 55 to 95 °C in different experiments), as well as full reversibility of the thermal unfolding in lipid-free apoC-1 (*16*), indicates that the observed values of T_R are not affected by the protein heat unfolding in our experiments and reflect the intrinsic ability of the proteins to form discoidal complexes with DMPC.

To correlate the heat-induced changes in the α-helical structure of the protein−DMPC complexes with the morphological changes in these complexes, we utilized dynode voltage measurements in CD experiments. Dynode voltage is a high voltage applied to the photomultiplier of the UV detector to compensate for the reduction in the light intensity resulting from the UV light scattering and/or absorption. In our earlier CD and EM studies of apoC-1−DMPC disks ($d \sim 17$ nm), we showed that the heat-induced changes in the dynode voltage at 222 nm, $V_{222}(T)$, result solely from the light scattering of the liposomes. We demonstrated that the heat-induced increase in the dynode voltage results from an increase in the particle size and/or refractive index that occurs upon lipoprotein fusion and formation of large and/or multilamellar DMPC vesicles (*16*). Thus, dynode voltage in CD experiments provides a useful tool to monitor heat-induced fusion of discoidal lipoproteins.

Figure 5 shows the dynode voltage data, $V_{222}(T)$, of DMPC complexes with Q31P and L34P that were recorded at 222 nm simultaneously with the CD data in Figure 4; similar data of R23P−DMPC disks (not shown) displayed low signal-to-noise ratio, apparently resulting from a less well-ordered protein conformation and hence a lower refractive index of the particles. The data in Figure 5 show a heat-induced growth in $V_{222}(T)$ that increases at slower heating rates. A similar trend observed in the dynode voltage data of WT−DMPC complexes indicates that the prolonged exposure to elevated temperatures leads to a formation of larger and/or multilamellar lipid vesicles (*16*). Furthermore, similar to the $\Theta_{222}(T)$ data in Figure 4, the $V_{222}(T)$ data in Figure 5 display hysteresis and show large scan rate effects on the heating curves. This further confirms that the heat-induced protein unfolding and the concomitant lipoprotein fusion [monitored by $\Theta_{222}(T)$ and $V_{222}(T)$, respectively] are irreversible transitions associated with high activation enthalpy.

Importantly, the cooling curves in Figure 5 show a steep reduction in $V_{222}(T)$ upon temperature decrease of the Q31P−DMPC samples below $T_R = 38 \pm 1.5$ °C and L34P−DMPC samples below $T_R = 33 \pm 1.5$ °C. Such a reduction in the dynode voltage (and thus the light scattering) must originate from the vesicle-to-disk conversion upon cooling that was detected by EM (*16*). The temperatures T_R of the disk reconstitution determined from the corresponding $\Theta_{222}(T)$ and $V_{222}(T)$ data in Figures 4 and 5 agree to better than 2 °C, which is within the accuracy of their experimental determination, confirming the consistency of our approach. In summary, the CD and the dynode voltage data in Figures 4

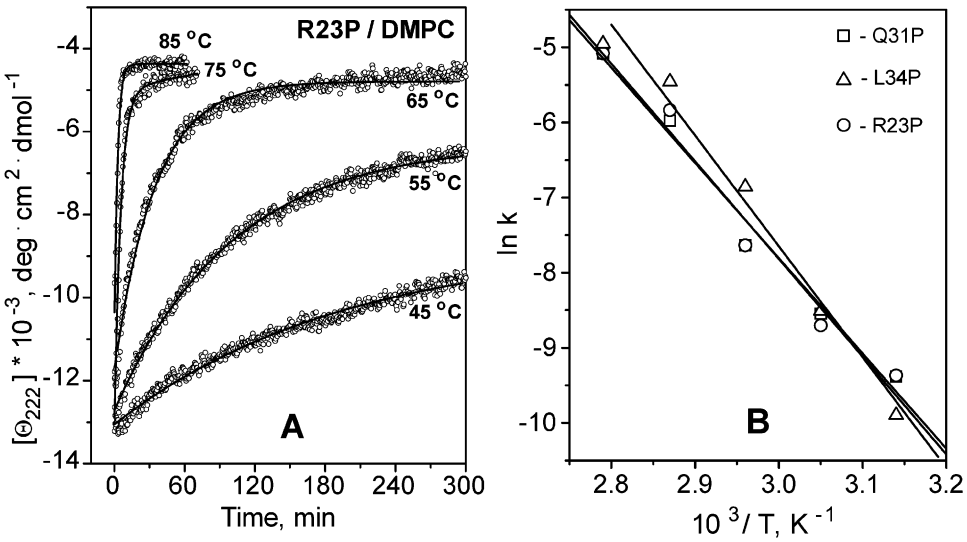

FIGURE 6: Thermal unfolding kinetics of the mutant apoC-1 on DMPC disks. (A) Time course of the R23P unfolding on the disks induced by temperature jumps from 25 to 45−85 °C and monitored by CD at 222 nm. Final temperatures are indicated on the lines. Solid lines show data fitting by single exponentials. (B) Arrhenius plot, ln $k(T)$ versus $1/T$, for the α-helical unfolding in DMPC complexes with Q31P (□), L34P (△), and R23P (○). The unfolding rates $k(T)$ were determined from single-exponential fitting of the CD data, $\Theta_{222}(t)$, recorded in T-jump experiments, such as that shown in panel A.

and 5 consistently show that the highest temperatures T_R of the disk reconstitution are significantly different for different apoC-1 mutants.

To determine the activation enthalpy ΔH^* and Gibbs free energy of activation, $\Delta G^* = \Delta H^* - T\Delta S^*$, for the denaturation of the mutant apoC-1−DMPC disks, we measured the rates of protein unfolding in these lipoproteins at different temperatures. The unfolding was induced by the temperature jumps from 25 to 45−85 °C and was monitored by CD at 222 nm. The kinetic data $\Theta_{222}(t)$ for R23P−DMPC complexes are shown in Figure 6A; the data for other mutants (not shown) are very similar. The unfolding rates $k(T)$ at various temperatures were determined for all mutant−DMPC complexes by single-exponential data fitting (solid lines in Figure 6A), and the Arrhenius activation energy E_a was determined from the slope of the Arrhenius plot, ln $k(T)$ versus $1/T$ (Figure 6B). Interestingly, the unfolding rates $k(T)$ and the activation energies E_a for the denaturation of DMPC complexes with Q31P, L34P, R23P, and WT are similar within the error of their experimental estimate, as indicated by the close overlap of the corresponding Arrhenius plots (Figure 6B). Consequently, the Gibbs activation energy ΔG^* of the apoC-1−DMPC disk denaturation (which is proportional to $-\ln k$) or its enthalpic component, $\Delta H^* \sim E_a$ (which is proportional to the slope of the Arrhenius plot) are not significantly altered by the Pro mutations analyzed in this work.

DISCUSSION

Structural and energetic parameters of the selected apoC-1 mutants and their complexes with DMPC are summarized in Table 1. First, the results in Table 1 show no correlation between the α-helical apolipoprotein content in solution and on the lipoproteins. For example, L34P in solution is substantially unfolded by the Pro substitution, yet its secondary structure on DMPC disks is identical to that of the WT and contains 65% α-helix. Such a high helical content suggests that the L34P substitution near the start position of the C-terminal α-helix in apoC-1 does not prevent the correct folding of both the N- and the C-terminal helices on the disk. In contrast, R23P substitution in the internal position of the N-terminal helix leads not only to a complete protein unfolding in solution but also to a large reduction in the protein helical content on the disk as compared to the WT−DMPC disks (Figure 3, Table 1). Such a reduced helical content of 40%, or about 23 amino acids, suggests that in R23P−DMPC disks only the C-terminal helix is folded while the N-terminal helix remains largely unfolded.

Second, the results in Table 1 show that the lipoprotein disk diameter does not correlate with the secondary protein structure in solution or on the disks. Indeed, despite substantially lower α-helix content in R23P−DMPC compared to WT−DMPC or L34P−DMPC disks, these disks have similar diameters. Furthermore, Q31P in solution and on the disk has α-helical content similar to that of the WT, yet Q31P−DMPC disks have significantly smaller diameters compared to those containing WT and other mutants. Such a difference in the disk diameter may result from the effect of the Q31P substitution in the interhelical turn region on the relative orientation of the α-helices at the disk circumference.

Importantly, our kinetic data show that the free energy barrier for the disk denaturation, ΔG^*, and its enthalpic component, $\Delta H^* \cong E_a$, are not significantly altered by the protein mutations analyzed in this work. This is evident from the close similarity in the thermal unfolding rates $k(T)$ of the DMPC complexes with WT and mutant apoC-1 and from the close superposition of the corresponding Arrhenius plots (Figure 6). This is a notable result, given the large variations in the protein helical content or the disk diameter exhibited by different mutant−DMPC complexes (Table 1). Such variations must significantly influence the protein−lipid interactions at the disk perimeter, yet, according to our data, they have no detectable effect on the kinetic stability of the lipoproteins. This suggests that the dominant contribution to the kinetic stability of discoidal lipoproteins comes from

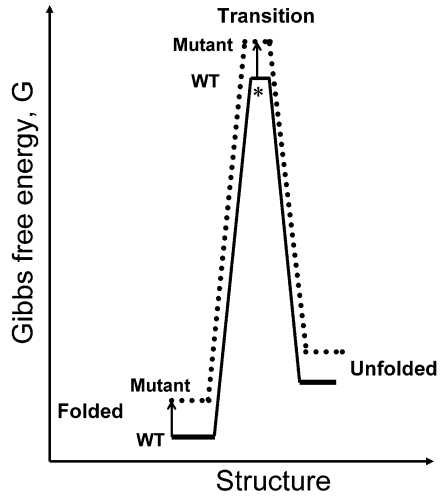

FIGURE 7: Free energy diagram illustrating mutational effects on the apoC-1−DMPC disk denaturation. The folded, transition (*), and unfolded states of the lipoproteins containing WT (—) and mutant apoC-1 (···) are indicated. The mutation-induced changes in the free energy of the folded and transition states (shown by arrows) are similar; thus the height of the free energy barrier $\Delta G^* = G^* - G_F$ is not affected by mutations, as evident from the close superposition of the Arrhenius plots for different mutants (Figure 6B). Similarity in the apparent melting temperatures T_m of different mutant−DMPC complexes (evident from the comparison of the corresponding melting curves in Figure 4) suggests similar apparent thermodynamic stability ΔG_{app} for these complexes.

the transient disruption of lipid−lipid interactions that, in contrast to the lipid−protein interactions, are not significantly affected by protein mutations.

Mutational analysis of the lipoprotein unfolding kinetics, such as that reported in this study, may provide an insight into the structure of the rate-limiting transition state in lipoprotein denaturation. Indeed, in similar studies of globular proteins, comparison of the kinetic data for the mutant and WT proteins indicates the extent to which the interactions disrupted in the mutant are maintained in the transition state (*33*, *34*). In our study, the absence of detectable mutation-induced changes in the activation free energy of unfolding, $\Delta G^* = G^* - G_F$, illustrated in Figure 7 means that the interaction energy of protein groups affected by mutation with the rest of the complex is the same in the native and in the transition state. Consequently, the activation free energy of unfolding does not depend on the relative orientation of the N- and C-terminal helices (which is likely affected by Q31P mutation) or the secondary structure in the N-terminal half of apoC-1 (which is largely unfolded in R23P but is largely helical in other protein−DMPC complexes). This implies that the free energy barrier for lipoprotein unfolding originates from the lipid interactions with the C-terminal α-helix and/or the lipid−lipid packing interactions that are present in the disk but are disrupted in the transition state.

In contrast to the similarity in the kinetic parameters of the disk denaturation, the disk reconstitution with different mutants is markedly different. Thermal refolding of the protein moiety monitored by CD (Figure 4) and the concomitant lipoprotein reconstitution monitored by light scattering (Figure 5) clearly show that the disk reconstitution with Q31P starts at a significantly higher temperature, T_R = 38 °C, than that with L34P (T_R = 33 °C) and R23P (T_R = 28 °C). Comparison with the temperature T_c = 24 °C of the liquid crystal-to-gel transition in DMPC at which the disk reconstitution is fastest (*19*) shows that R23P forms disks only in a narrow temperature range near T_c, while L34P and, especially, Q31P can clear DMPC vesicles and form discoidal lipoproteins in significantly broader temperature ranges. Interestingly, the rank order of the observed T_R values correlates with the protein helical content in solution (Table 1): T_R(Q31P) > T_R(L34P) > T_R(R23P) and α%(Q31P) > α%(L34P) > α%(R23P). This correlation suggests that the higher the helix content of an apolipoprotein in solution, the more readily it clears DMPC vesicles and forms disks.

In summary, our results indicate that the protein helical conformation in solution may facilitate reconstitution of discoidal lipoproteins from lipid vesicles, yet it does not affect the kinetic stability of the resultant disks. Furthermore, our results indicate that the differences in the disk diameter (from $\langle d \rangle$ =13−17 nm) or in the protein conformation on the disk (from 40% to 67% α-helix) may not affect the lipoprotein stability and suggest that the enthalpic barrier for the lipoprotein denaturation is dominated by the lipid−lipid rather than lipid−protein interactions.

REFERENCES

1. Mahley, R. W., Innerarity, T. L., Rall, S. C., and Weisgraber, K. H. (1984) Plasma lipoproteins: Apolipoprotein structure and function, *J. Lipid Res. 25*, 1277−1294.
2. Atkinson, D., and Small, D. M. (1986) Recombinant lipoproteins: implications for structure and assembly of native lipoproteins, *Annu. Rev. Biophys. Biophys. Chem. 15*, 403−456.
3. Brown, M. S., and Goldstein, J. L. (1976) Receptor-mediated control of cholesterol metabolism, *Science 191*, 150−154.
4. Fielding, C. J., and Fielding, P. E. (1995) Molecular physiology of reverse cholesterol transport, *J. Lipid Res. 36*, 211−228.
5. Krieger, M. (1999) Charting the fate of "good cholesterol": Identification and characterization of the HDL receptor SR-BI, *Annu. Rev. Biochem. 68*, 523−528.
6. Kunitake, S. T., Jarvis, M. R., Hamilton, R. L., and Kane, J. P. (1992) Binding of transition metals by apolipoprotein A-I-containing plasma lipoproteins: Inhibition of oxidation of low-density lipoproteins, *Proc. Natl. Acad. Sci. U.S.A. 89*, 6993−6997.
7. Segrest, J. P., Jones, M. K., De Loof, H., Brouillette, C. G., Venkatachalapathi, Y. V., and Anantharamaiah, G. M. (1992) The amphipathic helix in the exchangeable apolipoproteins: A review of secondary structure and function, *J. Lipid Res. 33*, 141−146.
8. Rye, K.-A., Clay, M. A., and Barter, P. J. (1999) Remodeling of high-density lipoproteins by plasma factors, *Arteriosclerosis 145*, 227−238.
9. Sparks, D. L., Frank, P. G., Braschi, S., Neville, T. A.-M., and Marcel, Y. L. (1999) Effect of apolipoprotein A-1 lipidation on the formation and function of pre-*β* and α-migrating LpA-I particles, *Biochemistry 38*, 1727−1735.
10. Suurkuusk, M., and Singh, S. K. (2000) Formation of HDL-like complexes from apolipoprotein A-I_m and DMPC, *Int. J. Pharmacol. 194*, 21−38.
11. Rye, K. A., and Duong, M. N. (2000) Influence of phospholipid depletion on the size, structure, and remodeling of reconstituted high-density lipoproteins, *J. Lipid Res. 41*, 1640−1650.
12. Cho, K.-H., Durbin, D. M., and Jonas, A. (2001) Role of individual amino acids of apolipoprotein A−I in the activation of lecithin: cholesterol acyltransferase and in HDL rearrangements, *J. Lipid Res. 42*, 379−389.
13. Sigalov, A. B., and Stern, L. J. (2001) Oxidation of methionine residues affects the structure and stability of apolipoprotein A−I in reconstituted high-density lipoprotein particles, *Chem. Phys. Lipids 113*(1−2), 133−146.
14. Braschi, S., Coffill, C. R., Neville, T. A., Hutt, D. M., and Sparks, D. L. (2001) Effect of acylglyceride content on the structure and function of reconstituted high-density lipoprotein particles, *J. Lipid Res. 42*, 79−87.
15. Gianazza, E., Eberini, I., Sirtori, C. R., Franceschini, G., and Calabresi, L. (2002) Size is a major determinant of dissociation

and denaturation behavior of reconstituted high-density lipoproteins, *Biochem. J. 366*, 245−253.
16. Gursky, O., Ranjana, and Gantz D. L. (2002) Complex of Human Apolipoprotein C-1 and Phospholipid: Thermodynamic or Kinetic Stability?, *Biochemistry 41*, 7373−7384.
17. Mehta, R., Gantz, D. L., and Gursky, O. (2003) Human plasma HDL are stabilized by kinetic factors, *J. Mol. Biol. 328*(1), 183−192.
18. Reijngoud, D.-J., and Phillips, M. C. (1982) Mechanism of dissociation of human apolipoprotein A-1 from complexes with DMPC as studied by guanidine hydrochloride denaturation, *Biochemistry 21*, 2969−2976.
19. Epand, R. M. (1982) The apparent preferential interactions of human plasma high-density apolipoprotein A-1 with gel-state phospholipids, *Biochim. Biophys. Acta 712*, 146−151.
20. Surewicz, W. K., Epand, R. M., Pownall, H. J., and Hui, S.-W. (1986) Human apolipoprotein A-I forms thermally stable complexes with anionic but not with zwitterionic phospholipids, *J. Biol. Chem. 216*(34), 16191−16197.
21. Jong, M. C., Hofker, M. H., and Havekes, L. M. (1999) Role of apoC-1 in lipoprotein metabolism: Functional differences between apoC1, apoC2, and apoC3, *Arterioscler. Thromb. Vasc. Biol. 19*, 472−484.
22. Shachter, N. S. (2001) Apolipoproteins C-I and C-III as important modulators of lipoprotein metabolism, *Curr. Opin. Lipidol. 12*, 297−304.
23. Streyer, E., and Kostner, G. M. (1988) Activation of lecithin: cholesterol acyltransferase by apolipoprotein D: comparison of proteoliposomes containing apolipoprotein D, A-1 or C-1, *Biochim. Biophys. Acta 958*, 484−491.
24. Jonas, A., Sweeny, S. A., and Herbert, P. N. (1984) Discoidal complexes of A and C apolipoproteins with lipids and their reactions with lecithin:cholesterol acyltransferase, *J. Biol. Chem. 259*, 6369−6375.
25. Rozek, A., Sparrow, J. T., Weisgraber, K. H., and Cushley, R. J. (1999) Conformation of human apolipoprotein C−I in a lipid-mimetic environment determined by CD and NMR spectroscopy, *Biochemistry 38*, 14475−14484.
26. Gursky, O., and Atkinson, D. (1998) Thermodynamic analysis of human plasma apolipoprotein C-1: High-temperature unfolding and low-temperature oligomer dissociation, *Biochemistry 37*, 1283−1291.
27. Gursky, O. (1999) Probing the conformation of human apolipoprotein C-1 by point mutations and trimethylamine-*N*-oxide, *Protein Sci. 8*, 2055−2064.
28. Gursky, O. (2001) Solution conformation of human apolipoprotein C-1 inferred from Pro mutagenesis: Far- and near-UV CD study, *Biochemistry 40*, 12178−12185.
29. Glasstone, S., Laidler, K. J., and Eyring, H. (1941) *The theory of rate processes*, McGraw-Hill, New York.
30. Gilmanshin, R., William, S., Callender, R. H., Woodruff, W. H., and Dyer, R. B. (1997) Fast events in protein folding: Relaxation dynamics of secondary and tertiary structure in native apomyoglobin, *Proc. Natl. Acad. Sci. U.S.A. 94*, 3709−3713.
31. Crane, J. C., Koepf, E. K., Kelly, J. W., and Gruebele, M. (2000) Mapping the transition state of the WW domain β-sheet, *J. Mol. Biol. 298*, 283−292.
32. Sanchez-Ruiz, J. M. (1992) Theoretical analysis of Lumry-Eyring model in differential scanning calorimetry, *Biophys. J. 61*, 921−935.
33. Fersht, A. R., Matouschek, A., and Serrano, L. (1992) The folding of an enzyme. I. Theory of protein engineering analysis of stability and pathway of protein folding, *J. Mol Biol. 224*, 771−782.
34. Serrano, L. (1994) Protein engineering and the dissection of protein folding pathways, *Curr. Opin. Struct. Biol. 4*, 107−111.

BI0341253